Indian Journal of Engineering & Materials Sciences
Vol. 13, August 2006, pp. 281-292

Effect of various stress ratio parameters on cold upset forging of irregular shaped billets using white grease as lubricant

K Baskaran & R Narayanasamy*

Department of Production Engineering, National Institute of Technology, Tiruchirappalli 620 015, India

Received 17 August 2005; accepted 3 March 2006

The aim of this study is to investigate the effect of various stress ratio parameters on cold upset forging of commercially pure aluminium solid billets of irregular shaped billets using white grease as lubricant applied on both sides. Samples with two different aspect ratios (ratio of height to diameter) namely, 0.5, 0.75 and 1.0, with different *b*/*a* ratios (ratio of minor to major diameter) namely 0.6 and 0.7 were prepared and cold forged. Cold deformation experiments were carried out in an incremental step and at the end of each step, dimensions such as height, contact and bulged diameters being measured. The calculations were made with the assumption that the radius of curvature of the barrel followed the form of a circular arc. Analysis of the experimental data showed that there exists a relationship between the measured barrel radius and various stress ratio parameters namely, (σ_θ/σ_z), (σ_m/σ_z), (σ_{eff}/σ_z), and (σ_m/σ_{eff}) developed under plane stress condition. An attempt has also been made to relate the percentage height reduction with respect to the stress ratio parameters namely, (σ_θ/σ_z), (σ_m/σ_z), (σ_{eff}/σ_z), and (σ_m/σ_{eff}) developed under plane stress condition and found to have an increasing trend with enhanced level of deformation.

IPC Code: B21J13/00, B23K20/00

The upsetting of solid cylinders is an important metal forming process and an important stage in the forging sequence of many products. Considerable attention has been devoted by Lee and Altan[1] to the analysis of influence of flow stress and friction on the metal flow in the upset forging of rings and cylinders considering the work hardening of material. Detailed studies of the deformation characteristics in axisymmetric upsetting such as geometric changes, stress and strains distributions were analysed by finite element method, as explained by Hartley *et al*[2]. Xue *et al.*[3] studied twist-compression forming by the finite element method. Further, it has been established by Landre *et al.*[4] when and where the fracture will take place during cold upsetting by utilization of ductile fracture criteria in conjunction with the finite element method. An approach to optimal design in forging is discussed by Castro *et al*[5]. In this, an evolutionary genetic algorithm is proposed to calculate the optimal work-piece shape geometry and work-piece temperature. For three-dimensional deformations in upset forging an admissible velocity field was proposed by Yang and Kim[6]. To analyze the upsetting of cylindrical billets between free falling tub and stationary anvil having unequal frictional properties, a relationship was developed between the applied load and the flow stress of the material for a cylinder under uniaxial compression by Avitzur[7]. Analysis of strain hardening for porous material under cold forging was also presented by Satsangi *et al.*[8], based on incremental and piecewise linear elastic-plastic finite element method. Further numerical methods are developed to determine the forging loads in order to solve forging problems, as explained elsewhere[9-11] namely, slab method, slip-line method and upper bound method. Also the existence of frictional constraints during upsetting between the dies and the work piece directly affects the plastic deformation of the latter, resulting in barrelling of the specimen as explained both experimentally and theoretically in the solid square billets of commercial aluminium by Manisekar and Narayanasamy[12].

The objective of current study is to study the effect of various stress ratio parameters on solid upset forging of commercially pure aluminium of irregular shaped billets with different aspect and *b*/*a* ratios. An attempt has also been made to investigate the influence of stress ratio parameters namely, (σ_θ/σ_z), (σ_m/σ_z), (σ_{eff}/σ_z), and (σ_m/σ_{eff}) respectively on different barrel radii namely major and minor axis and also on the percentage height reduction by using white grease as a die surface-billet lubricant.

*For correspondence (E-mail: narayan@nitt.edu)

Experimental Procedure

Cold upsetting specimens of 24 mm in diameter and of different heights corresponding to a set of aspect ratios (initial height to initial diameter ratio) namely 0.5, 0.75, and 1.0 were prepared by machining from 25 mm rods of commercially pure aluminium. These specimens were machined to different ratios of *b/a* (minor diameter/major diameter) namely 0.6 and 0.7.The cold upsetting of irregular shaped billets were conducted on a universal compression testing machine having capacity of 100 tons at room temperature with white grease as lubricant. For each test, nine specimens of the same dimensions were machined and deformed to different strain levels. The irregular shaped billets were upset between two flat platens. Extreme care is taken to place the specimens concentric with the axis of the platens. Before cold upsetting of the billets, the initial diameters such as major diameter ($D_{o\ major}$), minor diameter ($D_{o\ minor}$), initial height (h_o) of the specimens and the perimeter before deformation (P_o) were measured. After each incremental loading of deformation 3 metric tones the following parameters were measured: (i) Major top contact diameter ($D_{TC\ Major}$), (ii) Minor top contact diameter ($D_{TC\ Minor}$), (iii) Major bottom contact diameter ($D_{BC\ Major}$), (iv) Minor bottom contact diameter ($D_{BC\ Minor}$), (v) Major bulge diameter ($D_{B\ Major}$), (vi) Minor bulge diameter ($D_{B\ Minor}$), (vii) Height after deformation (h_f), (viii) Area for top contact surface (A_T), (ix) Area for bottom contact surface (A_B), (x) Perimeter for top contact surface (P_T), (xi) Perimeter for bottom contact surface (P_B), (xii) Major radius of curvature ($R_{m\ major}$) and (xiii) Minor radius of curvature ($R_{m\ minor}$).

The loads used for each deformation were recorded from the dial indicator of the universal compression testing machine. Major, minor contact diameters, bulge diameters, height before and after deformations were measured using a digital vernier caliper. Area, perimeter, bulge radius at each lubricated condition were recorded by scanning the irregular shaped billets using scanner. Further, the image was transferred to AutoCAD where the above said was measured. Fig. 1a shows the front view of the irregular shaped billet before deformation, where as Fig. 1b shows the shape after deformation. Figure 1c shows the photograph of undeformed irregular shaped billet samples of various heights. Figure 1d shows the photograph of deformed irregular shaped billet samples of various heights.

Theoretical

The mathematical expressions used and proposed for the determination of various upsetting stress parameters are discussed.

Radius of the barrel

As explained elsewhere[13], the expression for the circular radius of curvature of barrel is as follows:

$$R = \frac{x}{2} + \frac{h_f^2}{8x} \qquad \ldots(1)$$

where $x = (D_B - D_C)/2$. Since x is very small, the term $\frac{x}{2}$ can be neglected. Hence, Eq. (1) becomes

$$R = \frac{h_f^2}{4\,(D_B - D_C)} \qquad \ldots(2)$$

where, D_B is the bulge diameter, D_C is the contact diameter, and h_f is the height after deformation.

Uniaxial stress state condition

The mathematical expressions used and proposed for the determination of various upsetting parameters of upsetting for various stress state conditions are discussed here.

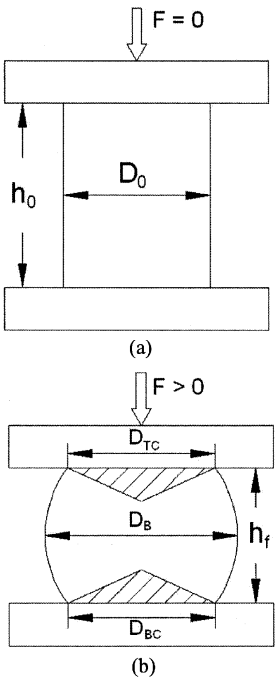

Fig. 1—Billet shape (a) before deformation and (b) after deformation

(c)

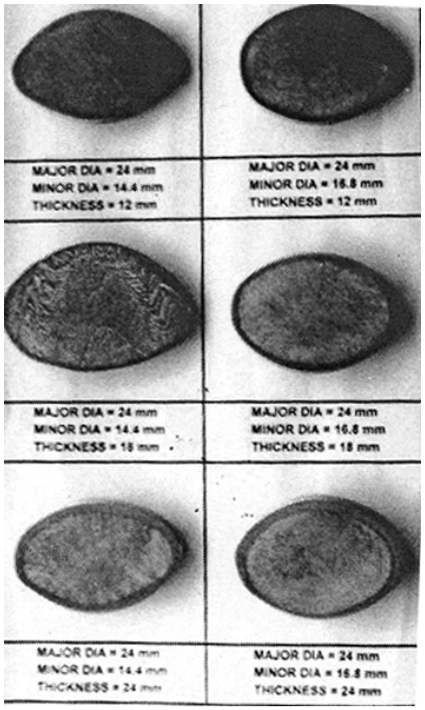

(d)

Fig. 1—Photograph of irregular shaped billet samples of aluminium for various height strains: (c) undeformed and (d) deformed

The state of stress in a homogeneous uniaxial compression process is as:

According to Abdel-Rahman *et al.*[14]

$$\sigma_z = -\sigma_{eff,} \quad \sigma_r = \sigma_\theta = 0 \qquad \ldots(3)$$

where, σ_z is the axial stress, σ_{eff} is the effective stress, σ_r is the radial stress, and σ_θ is the hoop stress.

Since $\sigma_\theta = \sigma_r = 0$ for uniaxial, the hydrostatic stress is given by:

$$\sigma_m = \frac{\sigma_z}{3} \qquad \ldots(4)$$

The axial strain is given as:

$$\varepsilon_z = \ln\left[\frac{h_0}{h_f}\right] \qquad \ldots(5)$$

The hoop stress is given as:

$$\varepsilon_\theta = \ln\left[\frac{P_b}{P_0}\right] \qquad \ldots(6)$$

where, ε_x is the axial strain, ε_θ is the hoop strain, P_b is the perimeter after deformation, and P_0 is the perimeter before deformation.

Plane stress state condition

According to Narayanasamy and Pandey[15], the state of stress in a plane stress state condition is as follows:

$$\sigma_{eff} = (0.5+\alpha)\left[3\left(1+\alpha+\alpha^2\right)\right]^{0.5}\sigma_Z \qquad \ldots(7)$$

where, ε_{eff} is the effective stress.

The axial stress is given as:

$$\sigma_z = \frac{\text{Load}}{A_C} \qquad \ldots(8)$$

where, σ_z is the axial stress, and A_C is the contact area.

Since $\sigma_r = 0$ at the free surface, it follows from the flow rule that;

$$\sigma_\theta = \left[\frac{1+2\alpha}{2+\alpha}\right]\sigma_z \qquad \ldots(9)$$

where, σ_θ is the hoop stress.

The Poisson's ratio is given as:

$$\alpha = \frac{\varepsilon_\theta}{2\ \varepsilon_z} \quad \ldots (10)$$

where, α is the Poisson's ratio.

Since the $\sigma_r = 0$ in case of plane stress condition, the hydrostatic stress is given as:

$$\sigma_m = \frac{\sigma_\theta + \sigma_z}{3} \quad \ldots (11)$$

The effective strain (ε_{eff}) is given as:

$$\varepsilon_{eff} = \left[\frac{2}{3}\left(\varepsilon_z^2 + \varepsilon_\theta^2 + \varepsilon_r^2\right)\right]^{0.5} \quad \ldots (12)$$

where, ε_z is the axial strain, ε_θ is the hoop strain and ε_r is the radial strain.

Here, ε_r and ε_θ are assumed to be equal for the determination of effective strain.

Various stress ratio parameters under plane stress state condition

Since the radial stress (σ_r) is zero at the free surface, it follows from the flow rule that:

$$\sigma_\theta = \left[\frac{1+2\alpha}{2\ +\alpha}\right]\ \sigma_z \quad \ldots (13)$$

where, σ_θ is the hoop stress, σ_z is the axial stress and α is the Poisson's ratio.

Eq. (13) can be written as:

$$\frac{\sigma_\theta}{\sigma_z} = \left[\frac{1+2\alpha}{2+\alpha}\right] \quad \ldots (14)$$

In the above equation, for the known values of α, the ratio $\frac{\sigma_\theta}{\sigma_z}$ can be determined.

Since the radial stress ($\sigma_r = 0$) at the free surface, the hydrostatic stress (σ_m) is given as:

$$\sigma_m = \frac{\sigma_\theta + \sigma_z}{3} \quad \ldots (15)$$

Eq. (15) can be written as:

$$\frac{\sigma_m}{\sigma_z} = (\sigma_\theta / \sigma_z)/3 \quad \ldots (16)$$

For the known values of $\frac{\sigma_\theta}{\sigma_z}$, the ratio $\frac{\sigma_m}{\sigma_z}$ can be determined.

The effective stress component (σ_{eff}) as explained elsewhere[16]

$$\sigma_{eff} = \left(0.5+\alpha\right)\ \left[3\ \left(1+\alpha+\alpha^2\right)\right]^{0.5}\ \sigma_Z \quad \ldots (17)$$

Eq. (17) can be written as:

$$\frac{\sigma_{eff}}{\sigma_z} = \left(0.5+\alpha\right)\left[3\left(1+\alpha+\alpha^2\right)\right]^{0.5} \quad \ldots (18)$$

In the above equation, for the known values of α, the ratio $\frac{\sigma_{eff}}{\sigma_z}$ can be determined.

From Eqs (7) and (11), the ratio of $\frac{\sigma_{eff}}{\sigma_z}$ can be determined.

$$\frac{\sigma_m}{\sigma_{eff}} = \frac{\left(\sigma_m / \sigma_{eff}\right)}{\left(\sigma_{eff} / \sigma_z\right)} \quad \ldots (19)$$

This section shows that stress ratio parameters like (σ_θ/σ_z), (σ_m/σ_z), (σ_{eff}/σ_z), and (σ_m/σ_{eff}) can be determined from dimensional output.

Results and Discussion

Figures 2-5 have been plotted between the measured radius and the various stress ratio parameters namely (σ_θ/σ_z), (σ_m/σ_z), (σ_{eff}/σ_z), and (σ_m/σ_{eff}) under plane stress condition for different aspect ratios (ratio of height to diameter), namely 0.5, 0.75 and 1.0 and for two different *b*/*a* ratios (ratio of minor diameter to major diameter) namely, 0.6 and 0.7. These plots have been made for the different barrel radii namely major and minor axis. The rate of change of barrel radius with respect to various stress ratio parameters is not same for all aspect ratios. This means that each aspect ratio has different slope. The barrel radius decreases very slowly with increasing stress ratio parameter in the case of higher aspect ratio when comparing with lower aspect ratios and the measured barrel radius remains almost constant, or

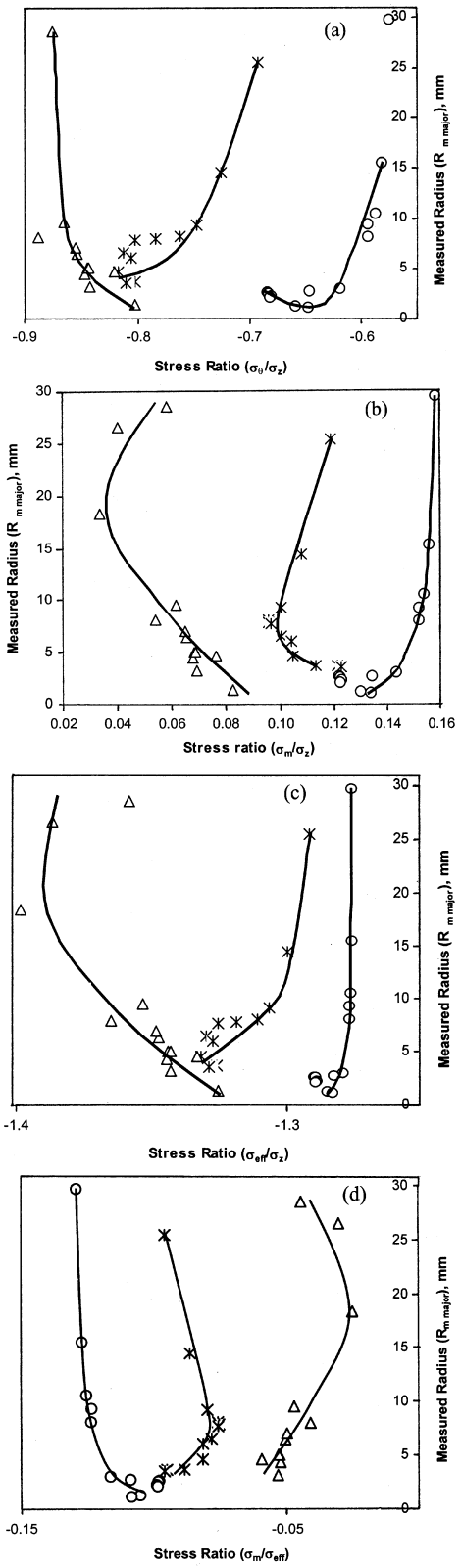

Fig. 2—Variation of measured radius (R_m major) with respect to the stress ratio (a) σ_θ/σ_z, (b) σ_m/σ_z, (c) σ_{eff}/σ_z and (d) σ_m/σ_{eff}, for b/a = 0.6 under plane stress condition [(∗) $h_0./d_0$=0.5, (Δ) $h_0./d_0$=0.75, (○) $h_0./d_0$=1.0]

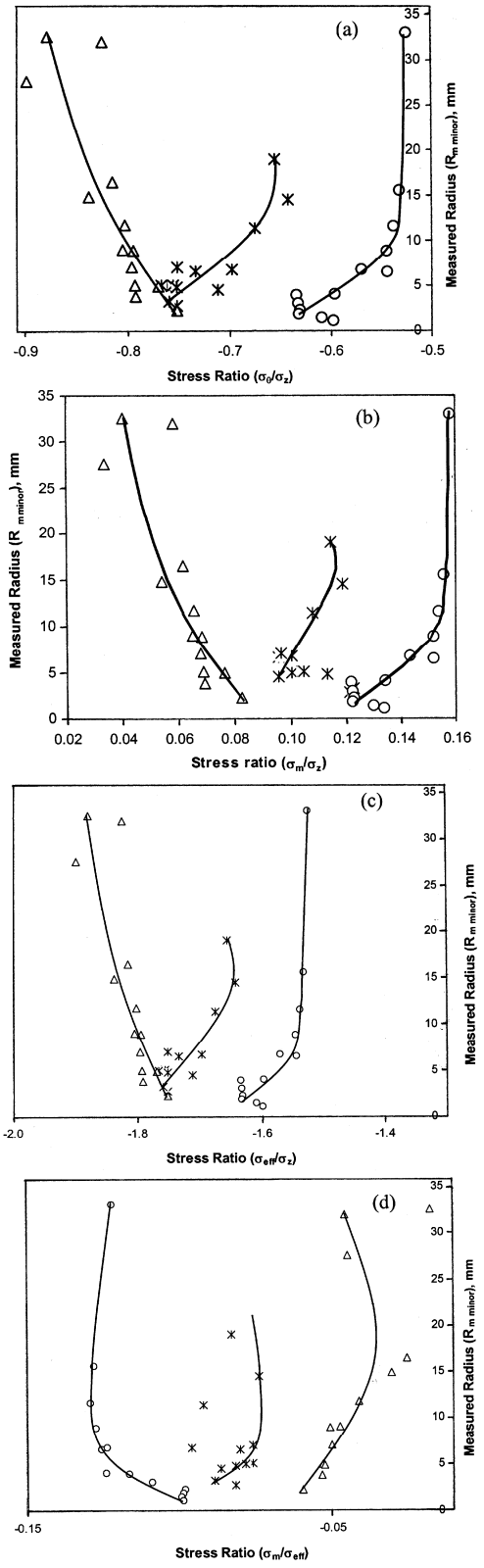

Fig. 3—Variation of measured radius (R_m minor) with respect to the stress ratio (a) σ_θ/σ_z, (b) σ_m/σ_z, (c) σ_{eff}/σ_z and (d) σ_m/σ_{eff}, for b/a = 0.6 under plane stress condition [(∗) $h_0./d_0$=0.5, (Δ) $h_0./d_0$=0.75, (○) $h_0./d_0$=1.0]

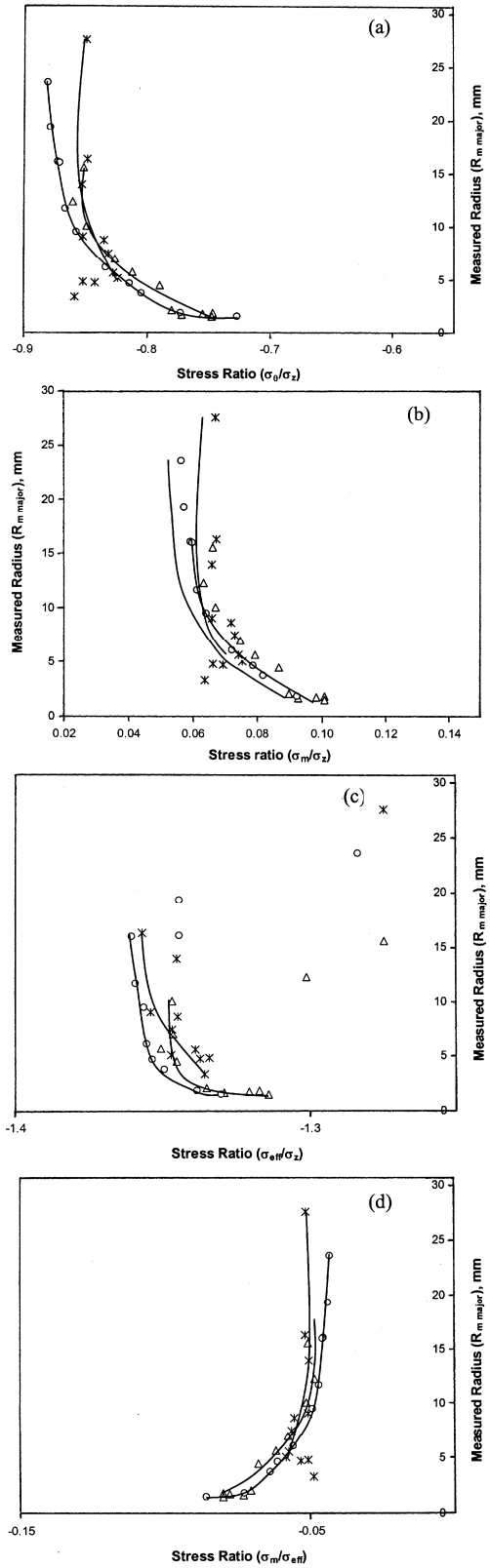

Fig. 4— Variation of measured radius (R_m major) with respect to the stress ratio (a) σ_θ/σ_z, (b) σ_m/σ_z, (c) σ_{eff}/σ_z and (d) σ_m/σ_{eff}, for b/a = 0.7 under plane stress condition [(∗) $h_0./d_0$=0.5, (Δ) $h_0./d_0$=0.75, (○) $h_0./d_0$=1.0]

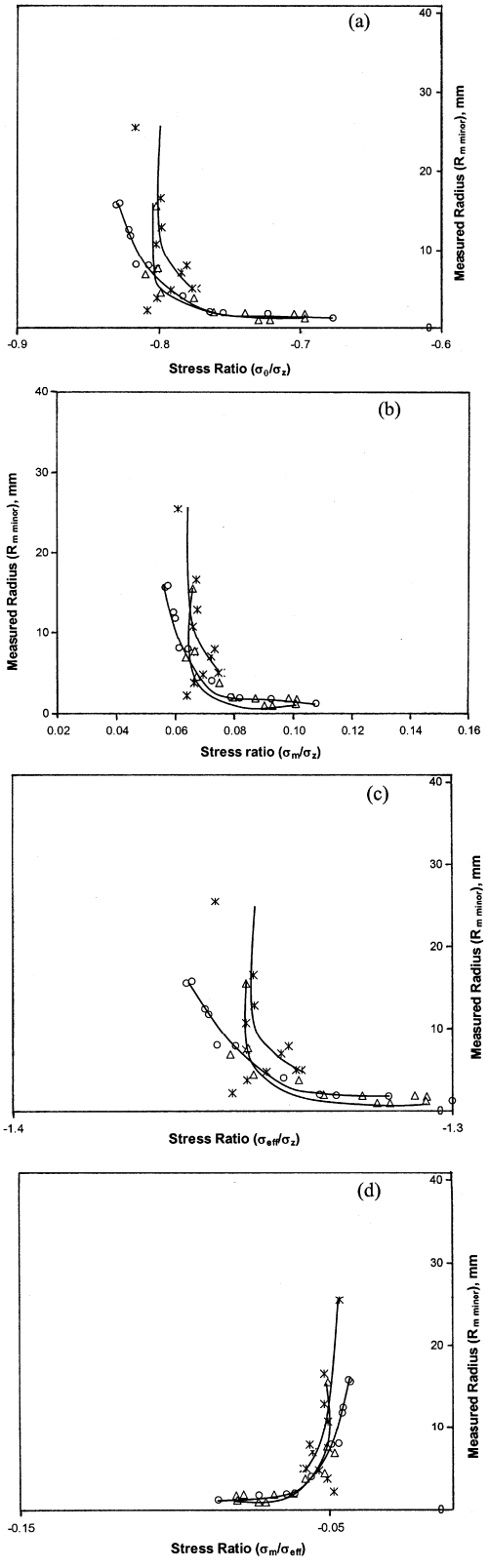

Fig. 5—Variation of measured radius (R_m minor) with respect to the stress ratio (a) σ_θ/σ_z, (b) σ_m/σ_z, (c) σ_{eff}/σ_z and (d) σ_m/σ_{eff}, for b/a = 0.7 under plane stress condition [(∗) $h_0./d_0$=0.5, (Δ) $h_0./d_0$=0.75, (○) $h_0./d_0$=1.0]

the radius of curvature decreases very slowly with increasing stress ratio parameter. This clearly indicated that, the rate of change of barrel radius with respect to the stress ratio parameters depends upon the ratio of b/a.

Figures 6-9 have been plotted between the natural logarithm of the radius of curvature of the barrel and the natural logarithm of the stress ratio parameters namely (σ_θ/σ_z), (σ_m/σ_z), (σ_{eff}/σ_z), and (σ_m/σ_{eff}) for plane stress stated condition for different aspect ratios and b/a ratios. These plots have been made for the different barrel radii (namely major axis and minor axis). These plots show that the rate of change of barrel radius with respect to the stress ratio parameter is different for different aspect ratios and b/a ratios. The variation in the slope value of the above straight lines is due to changes in shape of geometry.

Figures 10 and 11 have been plotted between the percentage height reduction and the various stress ratio parameters namely (σ_θ/σ_z), (σ_m/σ_z), (σ_{eff}/σ_z), and (σ_m/σ_{eff}) under plane stress condition for different aspect ratios and b/a ratios. For the increasing percentage height reduction, the stress ratio decreases rapidly in the case of higher aspect ratio when comparing with lower aspect ratio. This clearly indicates that there is a relationship between the percentage height reduction and stress ratio parameters.

Figures 12 and 13 have been plotted between the natural logarithm of the variation of percentage height reduction and the natural logarithm of the stress ratio parameters namely (σ_θ/σ_z), (σ_m/σ_z), (σ_{eff}/σ_z), and (σ_m/σ_{eff}) under plane stress condition for different aspect ratios and b/a ratios. The rate of change of height reduction with respect to the stress ratio is different for different aspect and (b/a) ratios.

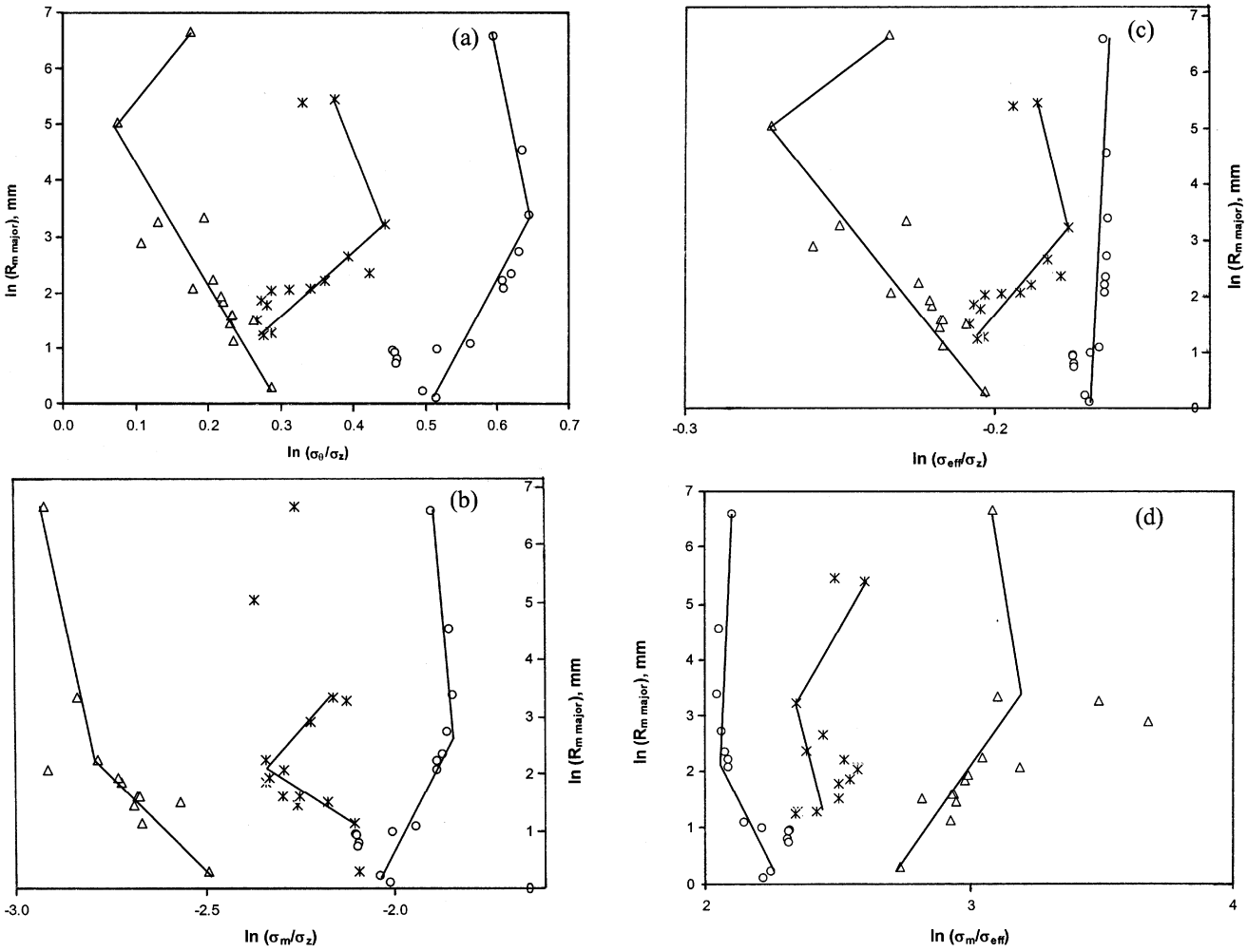

Fig. 6—ln Variation of measured radius (R_m major) with respect to the ln stress ratio (a) σ_θ/σ_z, (b) σ_m/σ_z, (c) σ_{eff}/σ_z and (d) σ_m/σ_{eff}, for b/a = 0.6 under plane stress condition [(×) $h_0./d_0$=0.5, (Δ) $h_0./d_0$=0.75, (○) $h_0./d_0$=1.0]

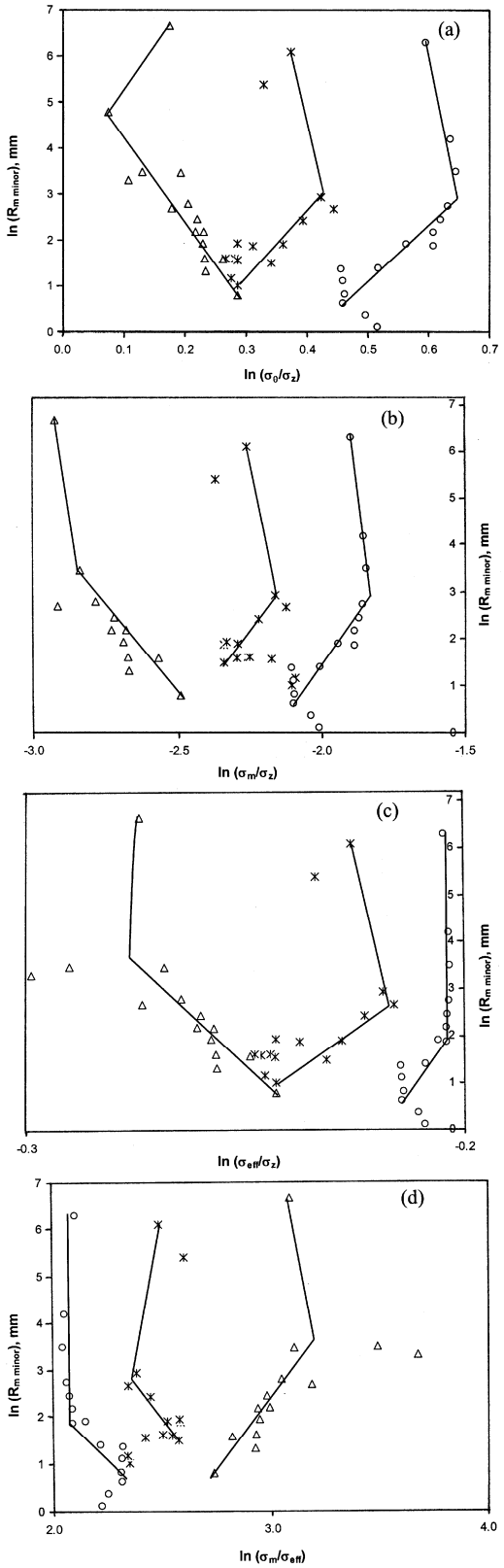

Fig. 7— ln Variation of measured radius (R_m minor) with respect to the ln stress ratio (a) σ_θ/σ_z, (b) σ_m/σ_z, (c) σ_{eff}/σ_z and (d) σ_m/σ_{eff}, for b/a = 0.6 under plane stress condition [(×) $h_0./d_0$=0.5, (Δ) $h_0./d_0$=0.75, (○) $h_0./d_0$=1.0]

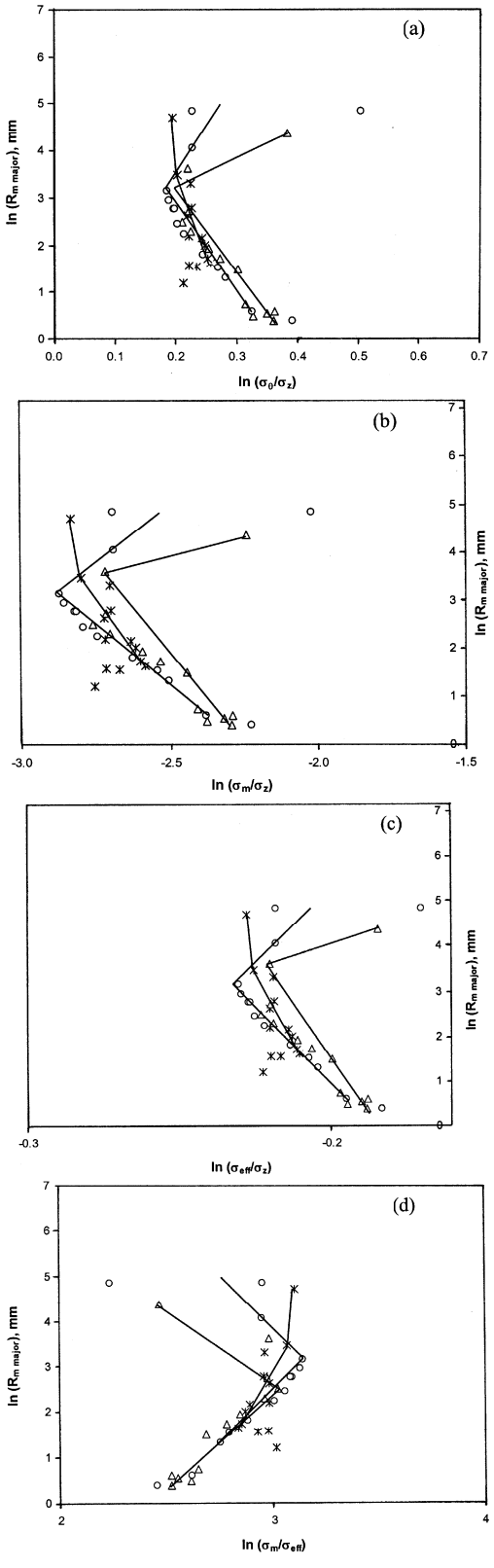

Fig. 8—ln Variation of measured radius (R_m major) with respect to the ln stress ratio (a) σ_θ/σ_z, (b) σ_m/σ_z, (c) σ_{eff}/σ_z and (d) σ_m/σ_{eff}, for b/a = 0.7 under plane stress condition [(×) $h_0./d_0$=0.5, (Δ) $h_0./d_0$=0.75, (○) $h_0./d_0$=1.0]

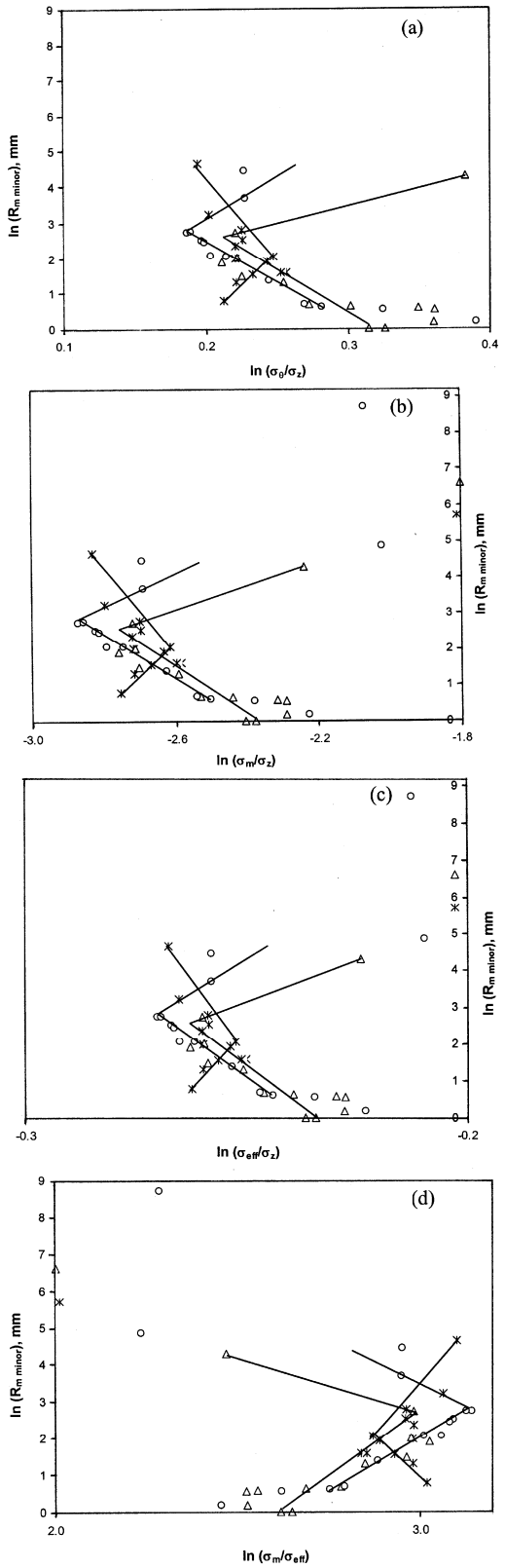

Fig. 9—ln Variation of measured radius (R_m minor) with respect to the ln stress ratio (a) σ_θ/σ_z, (b) σ_m/σ_z, (c) σ_{eff}/σ_z and (d) σ_m/σ_{eff}, for b/a = 0.7 under plane stress condition [(×) $h_0./d_0$=0.5, (Δ) $h_0./d_0$=0.75, (○) $h_0./d_0$=1.0]

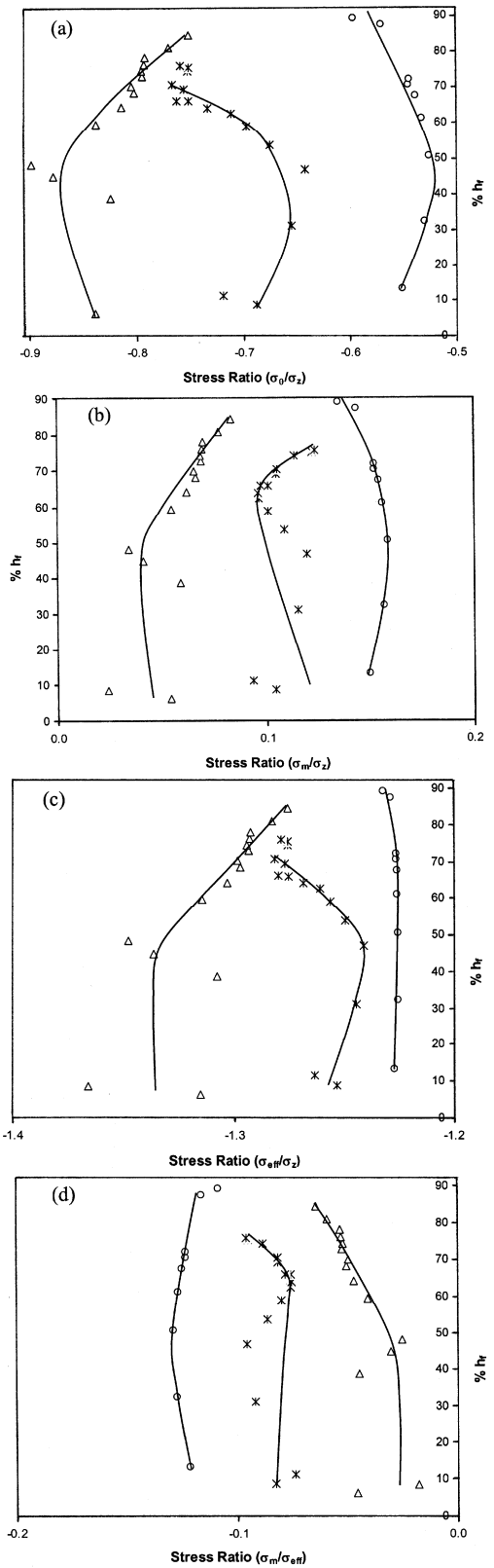

Fig. 10—Variation of percentage height reduction (h_f) with respect to the stress ratio (a) σ_θ/σ_z, (b) σ_m/σ_z, (c) σ_{eff}/σ_z and (d) σ_m/σ_{eff}, for b/a = 0.6 under plane stress condition [(×) $h_0./d_0$=0.5, (Δ) $h_0./d_0$=0.75, (○) $h_0./d_0$=1.0]

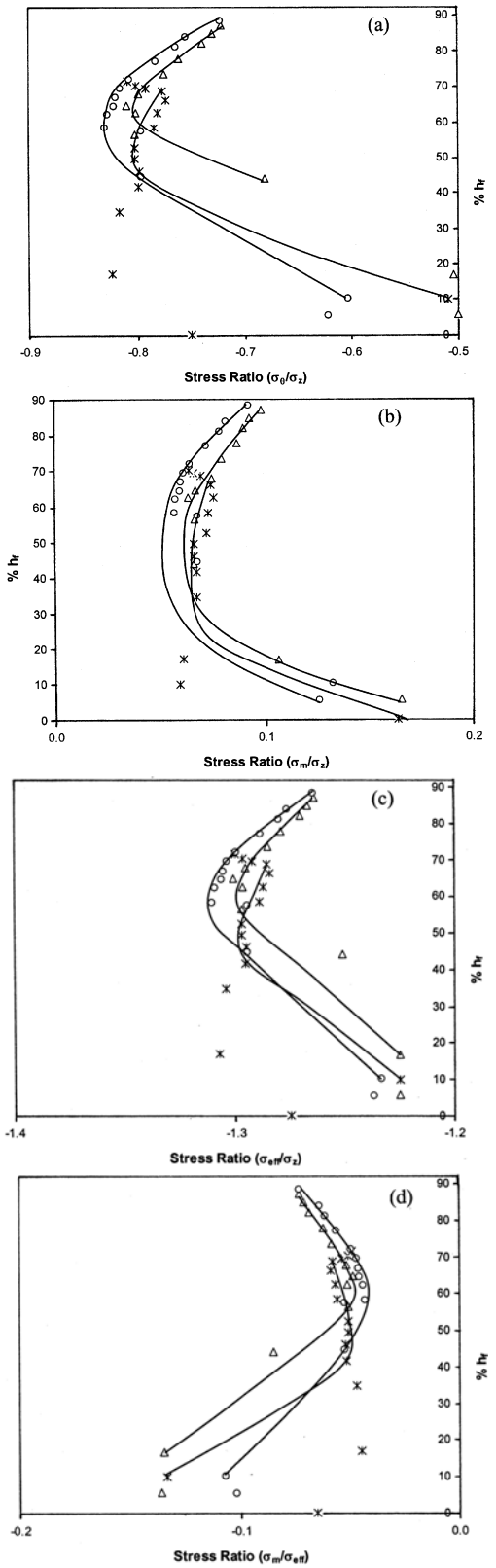

Fig. 11—Variation of percentage height reduction (h_f) with respect to the stress ratio (a) σ_θ/σ_z, (b) σ_m/σ_z, (c) σ_{eff}/σ_z and (d) σ_m/σ_{eff}, for b/a = 0.7 under plane stress condition [(×) $h_0./d_0$=0.5, (Δ) $h_0./d_0$=0.75, (○) $h_0./d_0$=1.0]

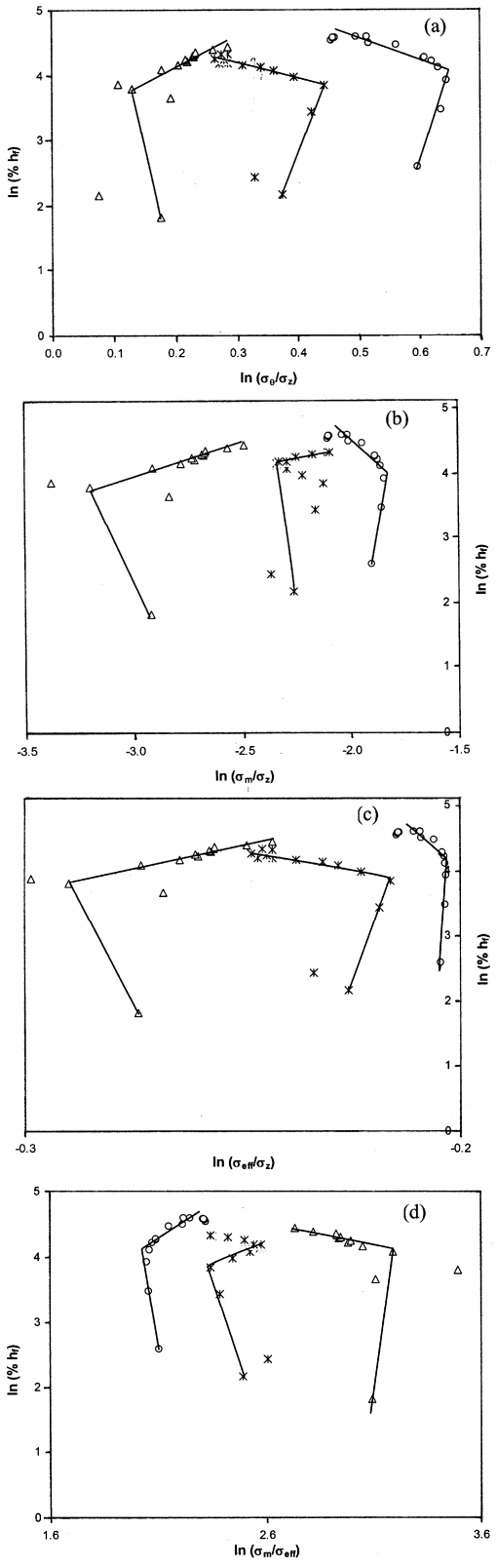

Fig. 12—ln Variation of percentage height reduction (h_f) with respect to the ln stress ratio (a) σ_θ/σ_z, (b) σ_m/σ_z, (c) σ_{eff}/σ_z and (d) σ_m/σ_{eff}, for b/a = 0.6 under plane stress condition [(×) $h_0./d_0$=0.5, (Δ) $h_0./d_0$=0.75, (○) $h_0./d_0$=1.0]

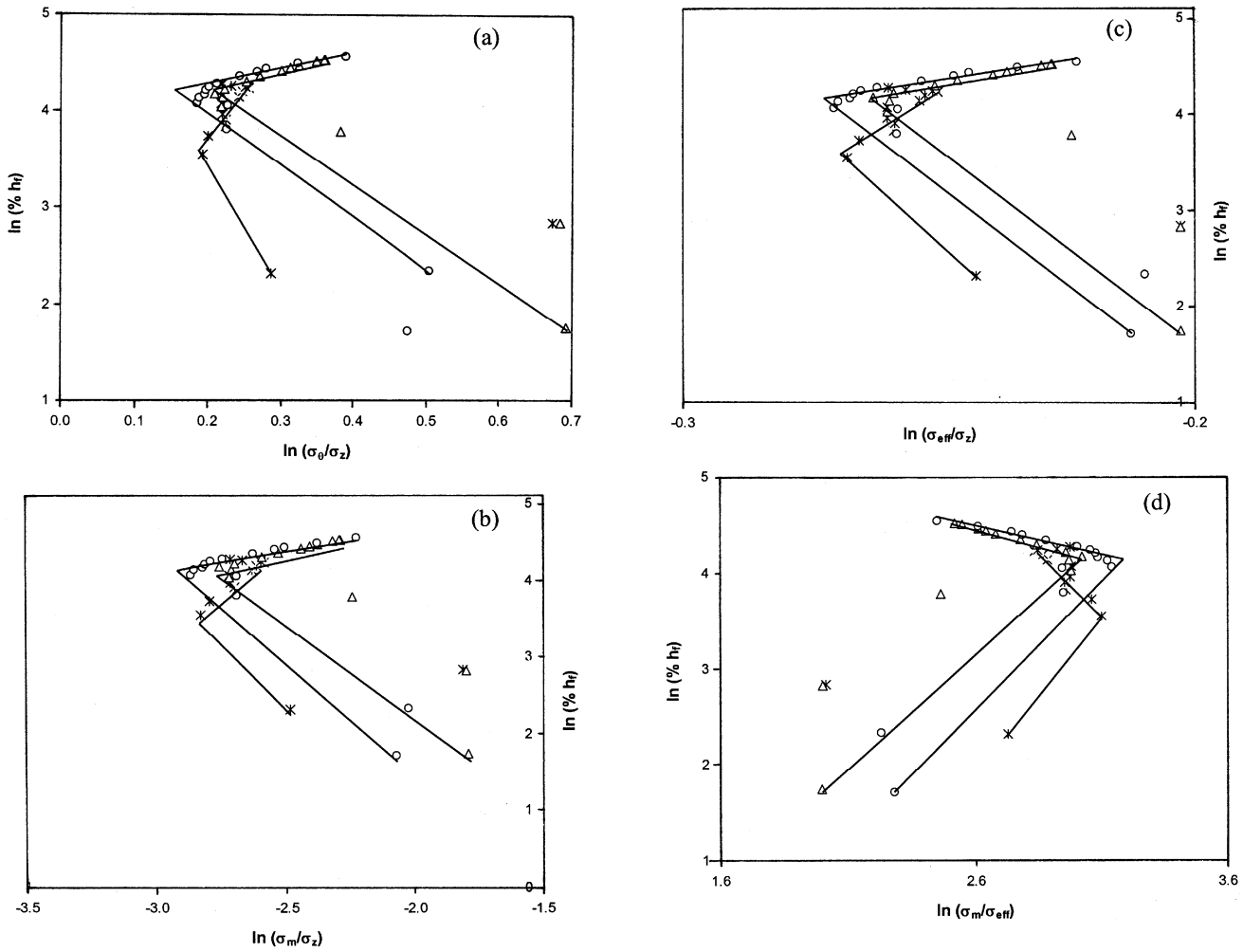

Fig. 13—ln Variation of percentage height reduction (h_f) with respect to the ln stress ratio (a) σ_θ/σ_z, (b) σ_m/σ_z, (c) σ_{eff}/σ_z and (d) σ_m/σ_{eff}, for b/a = 0.7 under plane stress condition [(×) $h_0./d_0$=0.5, (Δ) $h_0./d_0$=0.75, (○) $h_0./d_0$=1.0]

Conclusions

The following conclusions can be drawn from the present investigation:

(i) The rate of change of measured barrel radius with respect to the stress ratio parameter is very high for lower aspect ratio (ratio of height to diameter).

(ii) The rate of change of the percentage height reduction with respect to the stress ratio is different for different aspect ratios and b/a ratios.

(iii) A straight-line relationship is established between the natural logarithm of percentage height reduction and stress ratio parameter with one or two different slopes for each aspect ratio and b/a ratio.

Nomenclature

a = major diameter
b = minor diameter
F = force
h_0 = Initial height of the billet
D_0 = Initial diameter of the billet
h_f = height of the billet after deformation
D_B = bulge diameter of the billet after deformation
D_{TC} = top contact diameter of the billet after deformation
D_{BC} = bottom contact diameter of the billet after deformation

References

1 Lee C H & Altan T, *ASME Trans, J Eng Ind*, 94 (3) (1972) 775.

2 Hartley P, Sturgess C E N & Rowe G W, *Int J Mech Sci*, 22 (1980) 743-753.

3 Xue K M, Lu Y, Liu H H & Zhao X M, *Adv Technol Plasticity II*, (1993) 1065-1070.

4 Landre J, Pertence A, Cetlin P R, Rodrigues J M C & Martins P A F, *J Finite Elements Anal Design*, 39 (2003) 175-186.

5 Castro C F, Antonio C A C & Sousa L C, *J Mater Process Technol*, 146 (2004) 356-364.

6 Yang D Y & Kim J H, *Int J Mach Tool Des Res*, 26 (2) (1986) 147-156.

7 Avitzur B, *Metal Forming: Process and Analysis*, (McGraw-Hill Book Co., New York), 1968, 102-111.
8 Satsangi P S, Sharma P C & Prakash R, *J Mater Process Technol*, 136 (2003) 80-87.
9 Altan T, *Computer simulation to predict load, stress and metal flow in an axisymmetric closed die forging*, *Metal forming*, edited by Hoffmanner A L (Plenum Press, New York), 1971, 249-274.
10 Hill R, Lee E H & Tupper S J, *Trans ASME, J Appl Mech*, 73 (1951) 46-52.
11 Kudo H, *Int J Mech Sci*, 2 (1960) 102-127.
12 Manisekar K & Narayanasamy R, *Int J Adv Manf Technol*, 21 (2003) 84-90.
13 Malayappan S & Narayanasamy R, *J Mater Sci Technol*, 19 (2003) 1705-1708.
14 Abdel-Rahman M & El-Sheikh, *J Mater Process Technol*, 54 (1995) 97-102.
15 Narayanasamy R & Pandey K S, *J Mater Process Technol*, 70 (1997) 17-21.
16 Narayanasamy R, Senthil Kumar V & Pandey K S, *Mech Mater*, 38 (2006) 367-386.